Analyst

ROYAL SOCIETY OF CHEMISTRY

PAPER

View Article Online
View Journal | View Issue

Cite this: *Analyst*, 2025, **150**, 4781

A microfluidic sample preparation and droplet SERS detection all-in-one device for online analysis of deltamethrin in meat products

Jianying Huang,† Yayue Huang,† Ling Xia, Xiaohua Xiao* and Gongke Li *

Surface-enhanced Raman spectroscopy (SERS) is a powerful tool to acquire the fingerprint information of molecules rapidly, sensitively, and noninvasively. Its application in sample analysis, however, suffers from low repeatability due to the interference of the sample matrix. To address this issue, a microfluidic device was developed to realize all-in-one sample preparation and SERS detection for the online analysis of deltamethrin in meat products. This device was constructed using a microfluidic sample preparation unit and a droplet SERS detection unit. Through flow rate control, analytes at appropriate concentrations can be continuously encapsulated into online-generated microdroplets with SERS substrate Ag nanoparticle-coated Au nanoparticles. Stronger intensities with smaller relative standard deviations were observed by accumulating the Raman signals of microdroplets. Using the microfluidic SERS device, the enhancement factors of rhodamine 6G and deltamethrin were 2.7×10^7 and 3.8×10^5, respectively, with RSDs less than 4.0% (n = 19). Moreover, this device can be reused more than 7 times through simple cleaning procedures. The established microfluidic SERS analytical method has a linear range of 30.0–500 μg L^{-1} with a correlation coefficient of 0.9953, and the limit of detection was 11.6 μg L^{-1} (S/N = 3). The established microfluidic SERS method was applied to deltamethrin analysis in chicken skin, chicken and grass carp; 32.8 μg kg^{-1} of deltamethrin was found in the chicken skin sample. The accuracy and precision of the method were confirmed by high-performance liquid chromatography and recovery test results, indicating its potential for application in food safety.

Received 25th July 2025,
Accepted 17th September 2025

DOI: 10.1039/d5an00787a

rsc.li/analyst

Introduction

Surface-enhanced Raman spectroscopy (SERS) is a powerful tool for acquiring the fingerprint information of molecules rapidly and noninvasively.[1] Moreover, the localized surface plasmon resonance of metallic nanoparticles in SERS detection enhances sensitivity significantly.[2–4] However, the qualitative and quantitative analysis of analytes in complex samples, such as foods, suffers from low repeatability due to the interference of the sample matrix.[5] This unwanted interference from the sample matrix in SERS detection can be eliminated by sample preparation, which separates and concentrates the analytes from the original matrix, thereby making them applicable to be detected.[6] However, the time-consuming and labor-intensive conventional sample preparation methods extend the analysis duration dramatically and introduce additional systematic errors, which definitely offset the advantages of SERS.[7] To accelerate sample analysis and reduce sample transfer operation, a sample preparation and SERS detection all-in-one strategy has been proposed by our group.[8] For example, a $CoFe_2O_4$@HNTs/AuNPs substrate was developed to perform all-in-one magnetic solid-phase extraction and SERS detection for aromatic amines and nitrofuran analysis in fish feed and aquatic samples. In another work, a cell capture, Raman-silent probe labeling, and digital mapping all-in-one method was developed for *E. coli* analysis in beverages.[9] A porous 4-mercaptophenylboric acid@Ag foam chip and functionalized Raman-silent polymer were fabricated to realize *in situ* cell capture and Raman-silent signal generation. Beyond reducing analysis time, this sample preparation and SERS detection all-in-one strategy provides a selective, sensitive, stable, and practical SERS method for complex sample analysis.

The lab-on-a-chip system is another option to implement the all-in-one strategy of sample preparation and SERS detection.[10,11] Through customized microchip design and microfluidic control, sample preparation and SERS detection can be accomplished in sequence.[12–16] Ko *et al.*[17] fabricated a microfluidic dielectrophoresis-SERS microchip device to realize particle analyte enrichment and *in situ* SERS detection. Das *et al.*[18] integrated digital microfluidics with SERS detec-

School of Chemistry, Sun Yat-sen University, Guangzhou 510006, P.R. China.
E-mail: xiaoxhua@mail.sysu.edu.cn, cesgkl@mail.sysu.edu.cn
†These authors contributed equally to this work.

tion. By applying programming electrostatic potential control, their microchip can perform extraction, incubation, and SERS detection by droplet manipulation. Although rapid and sensitive, the operation of the microchip device is complicated, and the analysis throughput is limited for complex samples. A high-throughput droplet microfluidic platform was reported by Ho *et al.*[19] for cancer exosomes SERS detection, but the analyte and SERS-substrate have to be premixed before being injected into the microfluidic platform.

Deltamethrin is a widely used pesticide for sterilization in agricultural, livestock, and aquatic products.[20] Excessive residues of deltamethrin in food may induce cancer, blood diseases, and immune system disorders. Conventional methods for deltamethrin analysis are high-performance liquid chromatography,[21] mass spectrometry,[22] and fluorescence spectroscopy.[23] Although they offer accuracy and sensitive quantification of deltamethrin, these methods are time-consuming, expensive, and require specialized instrumentation. In contrast, SERS offers the advantage of rapid response, which is suitable for on-site food safety analysis.[24,25] To construct an accurate, sensitive, rapid, and practical deltamethrin analysis method, a microfluidic device was fabricated to realize sample preparation and SERS detection all-in-one, capable of online analysis of deltamethrin in meat products. Through flow rate control, analytes in appropriate concentrations after sample preparation can be continuously encapsulated into online-generated microdroplets with SERS substrate Ag nanoparticles-coated Au nanoparticle (Au@AgNPs). A microfluidic SERS method was then established using the device for deltamethrin analysis. The practicality of the method was verified by detecting deltamethrin in meat products.

Experimental

Materials and reagents

Polydimethylsiloxane (PDMS) prepolymer was purchased from CChip Scientific Instrument Co., Ltd (Suzhou, China). Silver nitrate, sodium citrate, ferric chloride hexahydrate ($FeCl_3{\cdot}6H_2O$), rhodamine 6G (Rh6G), rhodamine B (RhB), ascorbic acid, and ethylene glycol were purchased from Shanghai Aladdin Biochemical Technology Co., Ltd (Shanghai, China). Chloroauric acid ($HAuCl_4{\cdot}4H_2O$) was purchased from Shanghai Macklin Biochemical Co., Ltd. Deltamethrin was purchased from J&K Scientific Ltd (Beijing, China). *N*-Hexane, ethanol, methanol, and acetonitrile were all purchased from Guangzhou Chemical Reagent Factory (Guangzhou, China). Deionized water with a resistivity of 18.25 MΩ (Millipore, USA) was used for all experiments.

Instruments

Scanning electron microscope (SEM) images were captured using a Gemini 500 (Zeiss, Germany). The images of the microchannel were obtained using an epifluorescence microscope (Axio Observer Z1, Carl Zeiss AG, Germany). X-ray diffraction spectra (XRD) for various samples were obtained using a D8 X-ray spectrometer (Bruker, Germany). Raman signals were acquired using a portable Raman spectrometer (Model Inspector Raman, USA). The comparative analysis was conducted using high-performance liquid chromatography (Shimadzu 2010C, Japan). Simulations of the chip mixing capability and the electric field distribution were calculated by COMSOL Multiphysics 6.0 (COMSOL, Sweden). The fluorescence images were analysed using ImageJ software.

Microchip fabrication

PDMS was selected for the fabrication of the microchip, and the channel network was transferred by soft lithography. Briefly, a mixture containing curing agent and PDMS prepolymer in the ratio of 1 : 10 (w/w) was prepared, degassed, poured onto an SU-8 mold, and then cured at 90°C for 30 min.[26] Six connection holes were punched at the channel terminals. Next, microchannels were created by binding the PDMS channel layer with a glass slide after being treated with a plasma cleaner at 29.6 W for 1.5 min.

Au@AgNPs synthesis

To prepare the SERS substrate, 950 μL of $HAuCl_4{\cdot}4H_2O$ in 5 g L^{-1} was added to 60 mL of deionized water and boiled at 120°C for 1 min. Subsequently, 600 μL of sodium citrate solution (1%, w/v) was added rapidly, then stirred for 20 min until the solution turned purple-red. After cooling to room temperature, the solution containing the generated AuNPs was stored at 4°C for later use. To synthesize Au@AgNPs, 3 mL of the prepared AuNPs solution was measured and sonicated for 10 minutes. Next, 270 μL of ascorbic acid in 10 mmol L^{-1} was rapidly added to the AuNPs solution, followed by vortex stirring for 1.5 min. Afterward, 150 μL of $AgNO_3$ in 10 mmol L^{-1} was added dropwise with stirring at a controlled speed of 700 rpm for 20 min. Once the solution changed to orange-yellow from purple-red, the Au@AgNPs were formed by coating AgNPs onto AuNPs, according to a literature report.[27]

Microfluidic SERS operation

The sample or deltamethrin standard solution, and methanol were injected into the microchip device from inlets a and b, controlled by two syringe pumps, respectively, and the total flow rate at inlets a and b was fixed at 3.8 μL min^{-1}. An appropriate concentration gradient was generated by adjusting the flow rate percentage of the deltamethrin solution at inlet a. The coagulant $NaNO_3$ and Au@AgNPs solution were introduced from inlets d and e, respectively, at the flow rate of 3.8 μL min^{-1}. The total flow rate of the water phase at the droplet generation cross was 11.4 μL min^{-1}. Silicone oil containing 1% span 80 was selected as the oil phase and introduced into the microchip from inlet c, at a flow rate of 10.0 μL min^{-1}. A portable Raman spectrometer was used for microfluidic SERS analysis. During detection, a 785 nm laser source was focused on the detection unit of the microchip device for 10 s, and each trial was repeated three times. To recycle the device, the used microchip was washed three times with ethanol and

once with deionized water. After draining the liquid inside, the microchip can be sealed and stored for subsequent use.

The enhancement factor (EF) was calculated by using the following equation:[28]

$$\mathrm{EF} = \frac{I_{\mathrm{SERS}} \times C_{\mathrm{Raman}}}{I_{\mathrm{Raman}} \times C_{\mathrm{SERS}}} \quad (1)$$

where I_{SERS} and I_{Raman} refer to the Raman intensities of the characteristic peaks of the analyte measured on the microchip and silicon wafer, respectively. C_{SERS} and C_{Raman} refer to the concentrations of analyte injected into the microchip and onto the silicon wafer, respectively.

Results and discussion

Microchip device construction

To realize online sample preparation and deltamethrin SERS detection, a 50 mm long and 20 mm wide microchip device was designed and fabricated as shown in Fig. 1A. This device contains a microfluidic sample preparation unit and a droplet SERS detection unit. Fig. 1B shows that the microfluidic sample preparation unit contains three parts to execute sample concentration regulation (SP-I), SERS-active droplet generation (SP-II), and in-droplet sample incubation (SP-III). More detailed size information for each unit can be found in Fig. S1 in the SI. There are five inlets, a, b, c, d, and e, for sample solution, diluent, coagulant, and SERS substrate introduction, as well as an outlet, f, for waste discharge.

To perform microfluidic sample preparation, the sample solution and diluent were pumped into the microchip *via* inlets a and b, respectively. A sample in an appropriate concentration for SERS detection can be prepared online by adjusting the flow rate ratio of the sample solution and diluent. Once passed through the curved channel in SP-I, the well-mixed sample solution was driven into SP-II for SERS-active droplet generation. The coagulant $NaNO_3$ and Au@AgNPs solutions were introduced from inlets d and e, respectively, and converged with the sample solution at the droplet generation cross at a flow rate of 3.8 μL min^{-1} each and at 11.4 μL min^{-1} for the total water phase. The concentration of the coagulant $NaNO_3$ was optimized in a preliminary experiment to achieve the maximum SERS signal (as shown in Fig. S2 in the SI). Silicone oil containing 1% span 80 was introduced from inlet c at a flow rate of 10.0 μL min^{-1}. The flow rates for adjusting the sample concentration and droplet generation were confirmed by COMSOL (as shown in Fig. S3 in the SI). The sample solution, coagulant, and Au@AgNPs were encapsulated in a droplet and driven into the SP-III for in-droplet sample incubation. On passing through another curved channel in SP-III, the well-mixed sample-sensor all-in-one microdroplets were ready for Raman detection.

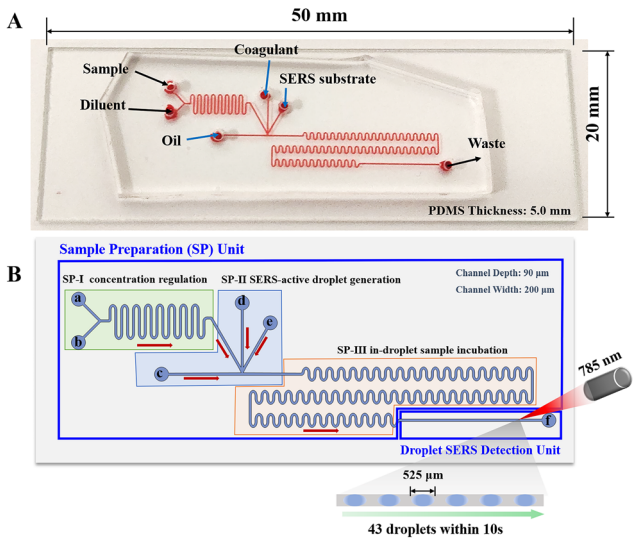

Fig. 1 A. Image of the microchip device for deltamethrin analysis. B. Schematic of microchip device construction for all-in-one microfluidic sample preparation and SERS detection.

In the SERS detection unit, a 785 nm laser source was focused on the detection unit of the microchip device for 10 s. Meanwhile, in the microchannel, multiple microdroplets were passing through the SERS detection point, accumulating the Raman intensity. Resembling conventional multiple parallel experiments, the integration of multiple microdroplets will provide more stable and repeatable SERS results.

As an important component, the SERS-active substrate Au@AgNPs were synthesized by the layer-by-layer growth method. The Au@AgNPs were characterized by TEM-EDS, UV, and XRD. The TEM diagrams (Fig. S4A in the SI) represent the uniform spherical appearance of Au@AgNPs. The EDS results (Fig. S3B in the SI) proved that there are Au, Ag, and other elements in the nanoparticles, which come from AuNPs, AgNPs, and silicon wafers. The particle size was 10–50 nm, and the average particle size was 27.1 nm (Fig. S3C in the SI). In the UV spectrogram (shown in Fig. S4A in the SI), there are two different surface plasmon resonance absorption peaks, which are mainly attributed to the surface plasmon resonance of the silver shell and gold core.[29] The electromagnetic field distribution of AuNPs and Au@AgNPs was simulated using COMSOL, as presented in Fig. S4D. The simulation result indicates that the electromagnetic field intensity around Au@AgNPs is significantly stronger than that around AuNPs. The core–shell structure of Au@AgNPs enables multiple surface plasmon resonance modes. Under laser excitation, these modes couple strongly with the incident light, leading to a pronounced localized surface plasmon resonance (LSPR) effect;[30] consequently, the SERS signal intensity is improved. The plasmon resonance effect exhibits its maximum intensity when the metal shell thickness is between 5 and 10 nm.[27] The crystal structures of AuNPs and Au@AgNPs were characterized by XRD. Au and Ag have very similar lattice constants, so their 2θ values are very close (as the results show in Fig. S5B in the SI). XRD patterns of Au@AgNPs showed sharper characteristic peaks than AuNPs, indicating that Ag nanostructures formed on the surface of Au seeds have higher crystallinity, and silver nanocrystals mainly grow along the (111) direction.[31]

Microfluidic sample preparation performance

To evaluate the sample preparation performance of the microchip device, the effectiveness of sample concentration regulation at SP-I, SERS-active droplet generation at SP-II, and in-droplet sample incubation at SP-III were investigated. To this end, 50 μg L^{-1} RhB solution and water were introduced into SP-I of the microchip from inlets a and b, respectively, with the total flow rate fixed at 3.8 μL min^{-1}. By adjusting the flow rate percentage of the RhB solution from 9.1%, 20%, 35%, 50%, 75% to 91%, the dynamic concentration gradient can be formed. An epifluorescence microscope was used to obtain the fluorescence images, and the COMSOL software was applied to simulate and reconstruct this dynamic nonlinear adjustment of sample concentration. According to the results of laboratory and simulation experiments shown in Fig. 2A and B, the precisely controllable sample solution can be achieved at the end of the SP-I of the microchip.

The droplet generation performance at SP-II was evaluated by introducing water from inlets a, b, d, e, and silicone oil from inlet c. A microscope having a high-speed camera was used to record the image of droplet generation. Both the channel width and the flow rate ratio affect the droplet generation.

By comparing the droplets generated in the microchip having various channel widths for water-phase flow (as shown in Fig. 2C and D, where W_w and W_o represent the water phase and the oil phase channel widths, respectively), the channel width ratio (water phase : oil phase) at 1 turned out to be optimal without droplet coalescence. This result was confirmed by the COMSOL simulation shown in Fig. S3A. Moreover, the flow rate of the water phase was adjusted from 1.4 to 20.0 μL min^{-1} to study the generation of droplets in the developed microchip. Both the microchip and simulation experiments provided an ideal water phase flow rate range of 10.0–12.5 μL min^{-1} for appropriately sized droplet generation with minimized oil phase (as shown in Fig. 2D and S3B, where Q_w and Q_o represent the flow rates at the water phase and oil phase channels, respectively). After setting the flow rates of the water phase and oil phase at 11.8 and 10.0 μL min^{-1}, respectively, the average number of droplets generated in 10 s for 10 batches was counted to be 43 with the relative standard deviation (RSD) of 2.5%, as shown in Fig. 2E. Moreover, by measuring the size of 33 generated droplets, an average length of 525 μm was obtained with RSD of 0.9%, presented in Fig. 2F. The uniformly sized droplets with precise controlled numbers generated by the SP-II of the microchip are the guarantee of the final SERS detection. Through precise control of the sample solution in SP-I and the controlled generation of droplets in SP-II, the analytes can be enriched within individual droplets. This enables stable and consistent droplet detection. Furthermore, sequentially generated droplets can be continuously and rapidly analysed, thereby enhancing detection stability.[32,33]

To obtain the maximum Raman intensity, the complete mixing of the analyte and the SERS substrate is required,[34]

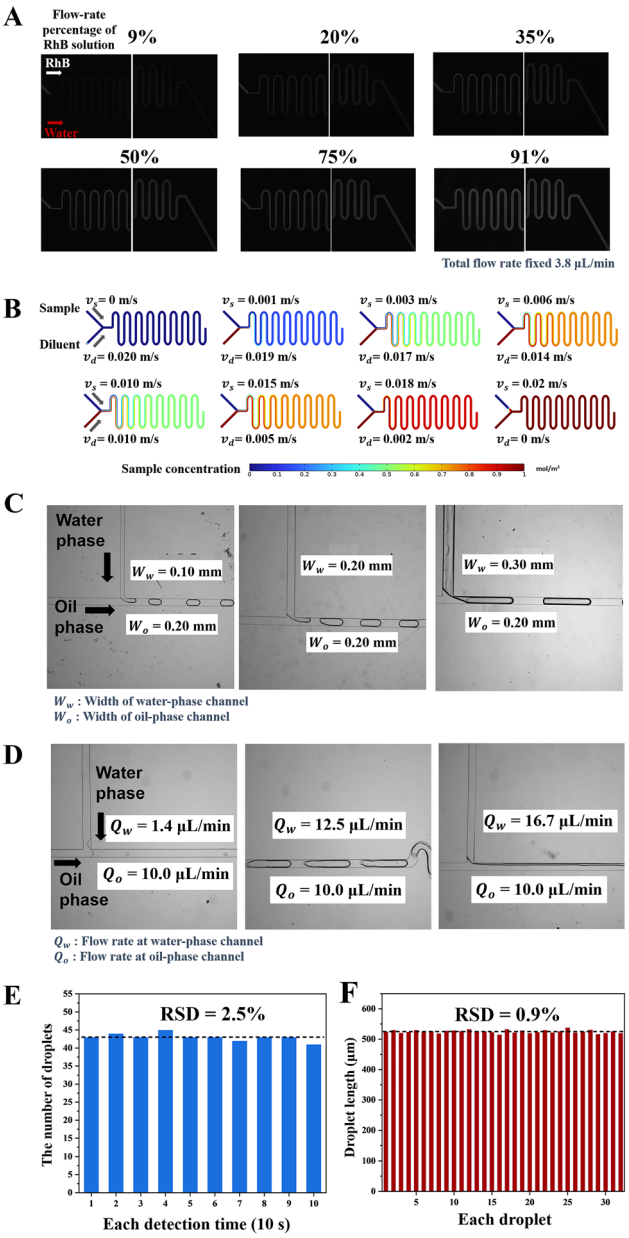

Fig. 2 Microfluidic sample preparation performance: A. fluorescence images of the entrance and the exit of SP-I in the sample preparation unit under different flow ratios of two phases. B. COMSOL-simulated concentration field in the concentration gradient generation zone under different flow rate ratios. C. Images of droplets generated in the device having a different width of the water-phase channel at SP-II of the sample preparation unit. D. Images of droplets generated under different flow rates at the water-phase channel at SP-II of the sample preparation unit. E. Statistics of droplet number generated within 10 s. F. Statistics of droplet length generated in the water-phase channel width of 0.2 mm at a flow rate of 11.8 μL min^{-1}.

especially when using Au@AgNPs. Therefore, the in-droplet sample incubation at SP-III was evaluated by introducing 50 μg L^{-1} of Rh6G at inlet a, and taking Raman detection at six locations, including four in the SP-III and the remaining two in the detection unit. On extending the mixing time in the

SP-III, the Raman intensity at 1512 cm^{-1} increased, which is the characteristic peak of Rh6G (shown in Fig. S6 in the SI). The similar high intensity recorded at the two locations in the Raman detection unit demonstrates the excellent mixing performance of the upstream process in SP-III of the microchip.

Microdroplet SERS detection performance

To confirm the presumptive gradient Raman signals by adjusting the sample concentration at SP-I of the sample preparation unit of the microchip, 100 μg L^{-1} Rh6G and water were continuously injected at inlets a and b, respectively. On setting the total flow rate at 3.8 μL min^{-1}, by adjusting the flow rate percentage of Rh6G from 10.0%, 16.5%, 25.0%, 50.0%, 75.0% to 100%, the concentration of Rh6G at the end of SP-I of the sample preparation unit should be 10, 16, 25, 50, 75 to 100 μg L^{-1}, respectively. The resulting Raman spectra are shown in Fig. 3A, and the intensities at the characteristic peak of Rh6G at 1512 cm^{-1} were increasing linearly (I_{1512} = 3965.2 log C_{Rh6G} + 447.5, r = 0.9985) with the gradient concentration of the sample generated by flow rate control.

The SERS activity of the microchip device was investigated by introducing the probe molecule Rh6G and the target analyte deltamethrin from the inlet individually, performing the detection at the SERS detection unit of the microchip. Fig. 3B shows the acquired Raman spectrum of Rh6G with a concentration of 10 g L^{-1} and 1.0 μg L^{-1} detection on a silicon wafer, using the microchip device with SERS substrate Au@AgNPs in the droplet. The Raman signal intensities at the characteristic peak of Rh6G at 1512 cm^{-1} were used for the enhancement factor (EF) calculation. An EF of 2.7 × 10^7 was achieved for Rh6G SERS detection using the microchip. Moreover, 1.0 μg L^{-1} deltamethrin was introduced into the microchip for online SERS detection. The obtained Raman spectrum is presented in Fig. 3C. The peaks at 855, 1001, 1040, 1129 and 1604 cm^{-1} correspond to the δ(C–H)oop, υring + δ(C–C)ip, δ(C–H)ip, υring, υ(C═C)ip, respectively, according to literature report.[35] The Raman detection of 10 g L^{-1} deltamethrin on silicon wafer was also performed and shown in Fig. 3C. An EF of 3.8 × 10^5 was calculated based on the intensities of the characteristic peak at 1040 cm^{-1}. The large EF values obtained in both Rh6G and deltamethrin SERS detection *via* the microchip proved its excellent SERS activity.

The stability of the microchip device was investigated by introducing 250 μg L^{-1} deltamethrin at inlet a, and acquiring Raman spectra at the droplet SERS detection unit at 19 detection points selected randomly. The recorded results were compared to the conventional method, which relies on manually mixing deltamethrin and Au@AgNPs solution before dropping them onto the silicon wafer for Raman detection. As shown in Fig. 3D, the average Raman intensity of 1.7 × 10^3 a.u. at 1040 cm^{-1} with RSD of 3.3% was observed using the microchip device, while an intensity of 1.3 × 10^3 a.u. with RSD of 6.6% was observed using a standard silicon wafer. This means that by replacing the silicon wafer with the developed microchip, a 30% Raman intensity enhancement with a half lower RSD can be achieved. After a simple cleaning operation, as stated in the Experimental section, the microchip can be reused for deltamethrin detection up to 7 times. Fig. 3E represents the average Raman intensity at 1040 cm^{-1}, and the RSD of 6.4% was calculated according to the 7-times usage on a single microchip,

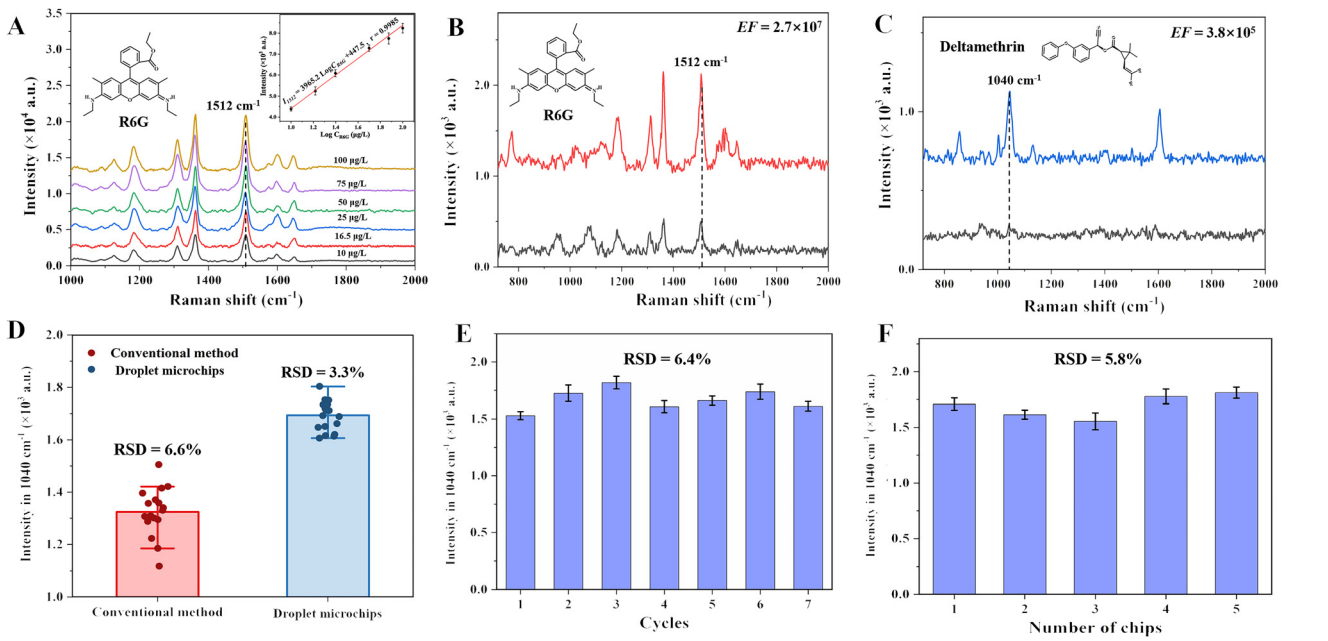

Fig. 3 Microdroplet SERS detection performance: A. SERS spectra of Rh6G in different concentrations and the linear fitting curve of SERS signals and concentration at 1512 cm^{-1}: I_{1512} = 3965.2 log C_{Rh6G} + 447.5, r = 0.9985. B. Calculations of EF values for Rh6G. C. Calculations of EF values for deltamethrin. D. Stability comparison of droplet SERS detection and off-chip conventional SERS detection of deltamethrin. E. Recyclability. F. Inter-microchip stability.

indicating good stability during reuse. Moreover, the inter-microchip stability was evaluated, and the results are exhibited in Fig. 3F. An RSD of 5.8% with an average Raman intensity at 1040 cm^{-1} detected using 5 different microchips was obtained, confirming the good inter-microchip stability.

Microfluidic SERS method for deltamethrin analysis

Before application in sample analysis, the selectivity and anti-interference performance of the microfluidic SERS method towards deltamethrin detection were investigated. To evaluate the selectivity, 500 μg L^{-1} of deltamethrin and the analogues of deltamethrin, including bifenthrin, cyhalothrin, permethrin, and carbendazim, were introduced into the microchip device, and online sample preparation and SERS detection were performed individually. The stronger Raman intensity, especially at the characteristic peak of deltamethrin at 1040 cm^{-1}, shown in Fig. 4A, demonstrates the good selectivity of the proposed deltamethrin detection method. The anti-interference performance was evaluated by mixing 300 μg L^{-1} of deltamethrin with possible interferents in meat samples, including glucose at 60 mg L^{-1}, sucrose at 60 mg L^{-1}, phenylalanine at 15 mg L^{-1}, arginine at 15 mg L^{-1}, lysine at 15 mg L^{-1}, vitamin B1 at 6.0 mg L^{-1}, valine at 6.0 mg L^{-1}, histidine at 6.0 mg L^{-1}, and a mixture of these. The Raman intensity at 1040 cm^{-1} exhibited no significant variation, as plotted in Fig. 4B, confirming the satisfactory anti-interference performance of the deltamethrin analysis method. The selectivity of Raman (SERS) detection was determined from both the distinct Raman fingerprints of different substances and the varying SERS responses on Au@AgNPs substrates.[36–39]

At optimized experimental conditions, the calibration curve of deltamethrin using the microfluidic SERS method was obtained. The total flow rate at inlets a and b was fixed to 3.8 μL min^{-1}, by adjusting the flow rate percentage of 500 μg L^{-1} deltamethrin from 6%, 8%, 10%, 20%, and 50% to 100%, the concentration of deltamethrin at the end of SP-I of the sample preparation unit should be 30, 40, 50, 100, and 200 to 500 μg L^{-1}, respectively. The Raman detection results in Fig. 4C provide a linear equation for deltamethrin, I_{1040} = 1332.4 log C_{DM} − 1390, in which I_{1040} is the signal intensity at 1040 cm^{-1}, and C_{DM} is the concentration of deltamethrin. The linear range of deltamethrin was 30.0–500 μg L^{-1} with a correlation coefficient r of 0.9953, and the LOD was 11.6 μg L^{-1} (S/N = 3). Moreover, the flow rate-adjustable continuous injection of the developed microfluidic device enables rapid concentration changes, accelerating the calibration curve acquisition.

This microfluidic SERS method was then applied in deltamethrin analysis in meat products, including chicken skin, chicken, and grass carp. After simple preprocessing, sample solutions were injected into the microchip device. The spiked recovery experiments were also performed. According to the results listed in Table 1, the recoveries of deltamethrin in meat samples are in the range of 80.2%–108% with RSDs less than 4.5% (n = 3), indicating the precision of the developed microfluidic SERS method. Moreover, 32.8 μg kg^{-1} of deltamethrin was detected in the chicken skin sample, as shown in Fig. 4D.

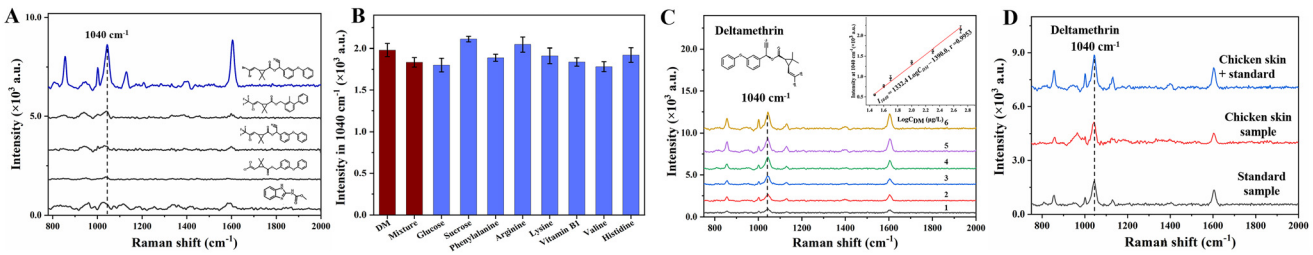

Fig. 4 Analytical performance of the microfluidic SERS method: A. selectivity; B. anti-interference; C. SERS response spectra of deltamethrin with different concentrations, and linear fitting curve of deltamethrin characteristic peak signal intensity and concentration logarithm: I_{1040} = 1332.4 log C_{DM} − 1390, r = 0.9953; D. SERS response spectra of deltamethrin in a deltamethrin standard sample, chicken skin sample, and chicken skin sample with deltamethrin standard sample.

Table 1 Detection and recovery of deltamethrin in samples

	The proposed method					
Samples	Find (μg kg^{-1})	Spiked (μg kg^{-1})	Recovery (μg kg^{-1})	RSD (%, n = 3)	HPLC method (μg kg^{-1})	Relative error (%)
Chicken skin	32.8(±1.9)	35.0	96.7	5.2	29.4	10.2
		70.0	108.0	3.6		
Chicken	n.d.	30.0	87.3	4.5	—	—
		60.0	102.1	3.9		
Grass carp	n.d.	30.0	80.2	3.8	—	—
		60.0	90.3	2.2		

n.d. = not detected.

Table 2 Method comparison for deltamethrin analysis

Samples	Sample preparation method	Detection methods	Linear range (mg L^{-1})	LOD (mg mL^{-1})	Ref.
Fish, chicken	Centrifugation	SERS	0.03–0.5	0.012	This work
—	—	SERS	0.03–5	0.011	35
Corydalis yanhusuo	Centrifugation and refrigeration	SERS	0.1–5	0.04	40
Water, serum	Centrifugation and filtration	Fluorescence	0.5–35	0.16	41
Apple juices	Filtration, evaporation, and redissolution	Luminescence	0.3–10	0.15	42
—	—	Colorimetric	6–35	0.58	43
Tomato	Filtration, rotary evaporation, and liquid–liquid extraction	GC	1–20	0.28	44

This result was confirmed by HPLC, with a relative error of 10.2%, which verified the accuracy of the developed microfluidic SERS method. The HPLC conditions are presented in Fig. S7 in the SI. Furthermore, by comparing with other deltamethrin analysis methods,[35,40–44] shown in Table 2, the microfluidic SERS method turns out to be a sensitive and practical method.

Conclusion

A microfluidic device enabling all-in-one sample preparation and SERS detection was fabricated to accomplish rapid, accurate, and sensitive deltamethrin analysis in meat products. By adjusting the flow rate, both the concentration of the analyte and the microdroplet generation can be controlled. When introducing Rh6G and deltamethrin into the microfluidic SERS device individually, the EF values were calculated to be 2.7×10^7 and 3.8×10^5, respectively, with RSDs less than 4.0% (n = 19). This device can be reused more than 7 times. A microfluidic SERS method was then established using the device for deltamethrin analysis, having a linear range of 30.0–500 μg L^{-1} (r = 0.9953) and the LOD of 11.6 μg L^{-1} (S/N = 3). On applying this method in meat product analysis, such as chicken skin, chicken, and grass carp, 32.8 μg kg^{-1} of deltamethrin was found in the chicken skin sample. Satisfactory recovery results were obtained in the range of 80.2%–108%, with the RSDs less than 5.2% (n = 3). These results were confirmed by the HPLC method, indicating the accuracy and precision of the proposed microfluidic SERS method. With the advantages in speed, accuracy, and sensitivity, this SERS method, along with the microfluidic device, has significant potential in food safety.

Author contributions

Huang Jianying: conceptualization, data curation, investigation, writing – original draft, data curation, visualization; Huang Yayue: writing – original draft, formal analysis, application of statistical, data curation, visualization, writing – original draft; Xia Ling: writing – review & editing; Xiao Xiaohua: funding acquisition, resources, supervision, writing – review & editing; Li Gongke: conceptualization, funding acquisition, project administration, resources, supervision, visualization, writing – review & editing.

Conflicts of interest

There are no conflicts to declare.

Data availability

The data supporting this article have been included as part of the supplementary information (SI). The SI includes the details and images of the experimental procedures mentioned in the article, such as device structure design, COMSOL simulations, characterizations of Au@AgNPs, and comparison with the HPLC method. Supplementary information is available. See DOI: https://doi.org/10.1039/d5an00787a.

Acknowledgements

The work was financially supported by the State Key Program of National Natural Science of China (No. 22134007), the National Natural Science Foundation of China (No. 22376225 and 22576240), and the Guangdong Basic and Applied Basic Research Foundation of China (No. 2024A1515011077), respectively.

References

1 Y. Liu, S. Gou, L. Qiu, Z. Xu, H. Yang, S. Yang and Y. Zhao, *Analyst*, 2024, **149**, 4343–4350.
2 H. Lai, Z. Yu, G. Li and Z. Zhang, *J. Chromatogr. A*, 2022, 463181.
3 J. Jin, Z. Guo, D. Fan and B. Zhao, *Mater. Horiz.*, 2023, **10**(4), 1087–1104.
4 Y. Mu, J. Islam, R. Murray, C. Larrigy, A. Russo, X. Zhang, A. J. Quinn and D. Iacopino, *Analyst*, 2023, **148**, 3087–3096.
5 Z. Chen, L. Yu, Z. Zhang, L. Su and Y. Xiong, *ACS Food Sci. Technol.*, 2024, **4**(2), 373–381.
6 J. Dong, G. Li and L. Xia, *Anal. Chem.*, 2022, **94**, 16901–16909.
7 J. Shi, C. Li and Z. Jiang, *Microchem. J.*, 2024, **196**, 109573.
8 H. Zhang, H. Lai, X. Wu, G. Li and Y. Hu, *Anal. Chem.*, 2020, **92**(6), 4607–4613.
9 L. Yin, B. Huo, L. Xia and G. Li, *Anal. Chem.*, 2024, **96**, 11036–11043.
10 Q. Zhang, S. Feng, L. Lin, S. Mao and J. Lin, *Chem. Soc. Rev.*, 2021, **50**, 5333.

11 G. Xing, J. Ai, N. Wang and Q. Pu, *Trends Anal. Chem.*, 2022, **157**, 116792.
12 Y. Cai, R. Sun, Y. Ren and Y. Gou, *Microchem. J.*, 2025, **211**, 113101.
13 C. Wang, G. Weng, J. Li, J. Zhu and J. Zhao, *Anal. Chim. Acta*, 2024, **1296**, 342291.
14 J. Liu, T. An, J. Peng, Q. Zhu, H. Zhao, Z. Liang, K. Mo, T. Liu and K. Wu, *Analyst*, 2025, **150**, 1151–1157.
15 Z. Sun, Y. Zhao, Y. Liu, C. Chen and H. Chen, *Analyst*, 2024, **149**, 5563–5571.
16 Z. Zuo, J. Pan and Q. Fang, *Talanta*, 2022, **249**, 123585.
17 K. Ko, H. Yoo, S. Han, W. S. Chang and D. Kim, *Analyst*, 2024, **149**, 5649.
18 A. Das, S. Fehse, M. Polack, R. Panneerselvam and D. Belder, *Anal. Chem.*, 2023, **95**, 1262–1272.
19 K. H. W. Ho, H. Lai, R. Zhang, H. Chen, W. Yin, X. Yan, S. Xiao, C. Y. K. Lam, Y. Gu, J. Yan, K. Hu, J. Shi and M. Yang, *ACS Sens.*, 2024, **9**, 4860–4869.
20 P. B. Carneiro and B. K. Bastos, *Food Chem.*, 2022, **380**, 132165.
21 H. Jiang, X. Bi, X. Huang, X. Guo, Z. Zou, Y. Li, X. Jing and J. Wu, *Acta Chromatogr.*, 2023, **35**(1), 21–27.
22 A. Batool, N. AlMasoud, Z. Nazar, H. Ullah, M. Sajid, T. S. Alomar, M. A. Khan, H. M. Asif, S. Iram, L. Ullah and S. Hussain, *Microchem. J.*, 2024, **200**, 110312.
23 D. Diery, T. D. Diegane, S. Diegane, D. P. Abdoulaye, K. Khemesse, M. O. M. Aly, S. S. Omar, G. M. Diabou, G. Philippe and C. Atanasse, *Int. J. Environ. Anal. Chem.*, 2022, **102**(17), 5445–5456.
24 Y. Shi, Y. Zhu, J. Sun, H. Yin and J. Yin, *Analyst*, 2024, **149**, 5041–5051.
25 C. Zhang, J. Zhu, W. Ye, X. Liu, R. Zhuo, C. Wang, H. Liu and W. Zhang, *Analyst*, 2025, **150**, 1122–1130.
26 J. Dong, G. Li, L. Xia and H. Li, *J. Chromatogr. A*, 2023, 464021.
27 S. Li, J. Chen, W. Xu, B. Sun, J. Wu, Q. Chen and P. Liang, *Mater. Chem. Front.*, 2023, **7**(6), 1100–1109.
28 X. Xu, K. Kim, H. Li and D. L. Fan, *Adv. Mater.*, 2012, **24**(40), 5401–5511.
29 H. Lai, G. Li and Z. Zhang, *Anal. Chim. Acta*, 2023, **1259**, 341159.
30 L. He, P. He, J. Li, M. Xiong, Y. Zhang and H. Yan, *J. Food Compos. Anal.*, 2025, **137**, 106856.
31 W. Liu, Z. Wang, Z. Liu, J. Chen, L. Shi, L. Huang, Y. Liu, S. Cui and X. He, *ACS Sens.*, 2023, **8**(4), 1733–1741.
32 X. Lin, F. Lei, X. Liang, Y. Jiao, X. Zhao, Z. Li, C. Zhang and J. Yu, *Opto-Electron. Adv.*, 2025, **8**, 240260.
33 H. Sun, Y. He, S. Qiao, Y. Liu and Y. Ma, *Opto-Electron. Sci.*, 2024, **3**, 240013.
34 S. Yue, J. Fang and Z. Xu, *Biosens. Bioelectron.*, 2022, **198**, 113822.
35 Z. Hu, D. Peng, F. Xing, X. Wen, K. Xie, X. Xu, H. Zhang, F. Wei, X. Zheng and M. Fan, *Molecules*, 2023, **28**, 17004.
36 Y. Song, K. Xiao, Q. Chen, X. Zhang, Z. Yu, W. Chen, X. Zhang, D. Zhang, D. Ni and P. Liang, *Chemosensors*, 2023, **11**(2), 73.
37 H. Li, C. Ren, J. Meng, Y. Gao, T. Ren, Y. Li, Y. Qiao, C. Liu and G. Che, *ChemistrySelect*, 2020, **5**, 6475–6481.
38 P. Tao, Y. Luo, K. Zheng, J. Cao, L. Zhu, X. Wang, W. Zhang, S. Dai, Q. Zou and P. Zhang, *Anal. Chim. Acta*, 2025, **1341**, 343646.
39 X. Ren, X. Feng, X. Li and X. Li, *Chem. Pap.*, 2021, **75**, 6477–6485.
40 H. Zhang, P. Nie, Z. Xia, X. Feng, X. Liu and Y. He, *Molecules*, 2020, **25**(18), 4081–4088.
41 J. R. Bhamore, S. Jha, R. K. Singhal, Z. V. P. Murthy and S. K. Kailasa, *Sens. Actuators, B*, 2019, **281**(11), 812–820.
42 I. A. Yahyai, J. Hassanzadeh and H. A. J. Al-Lawati, *Sens. Actuators, B*, 2021, **327**(7), 12892.
43 J. Zhu, L. Yin, W. Zhang, M. Chen, D. Feng, Y. Zhao and Y. Zhu, *Coatings*, 2022, **12**(1), 38–48.
44 A. E. A. E. Albadri, A. A. Elbashir, H. E. Ahmed, I. A. M. Mihaina and H. Y. Aboul-Enein, *Food Anal. Methods*, 2012, **5**(6), 1296–1302.